3
Singularities at interfaces

J. Eggers

School of Mathematics
University of Bristol
University Walk
Bristol BS8 1TW
United Kingdom

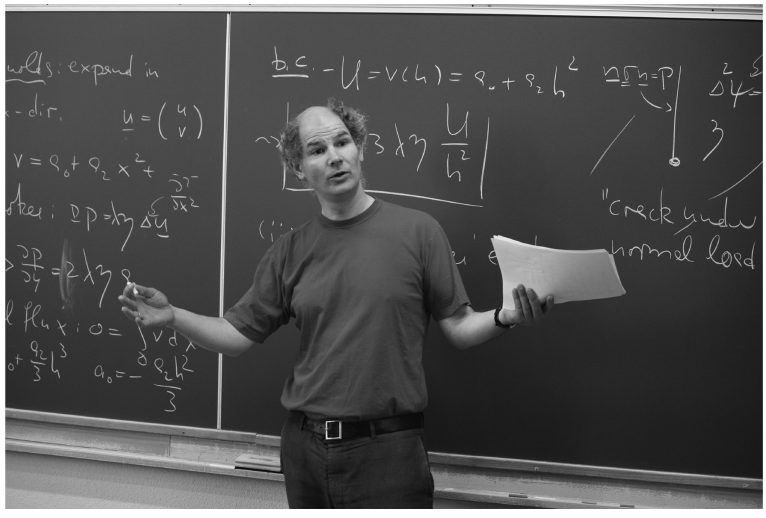

Soft Interfaces. Lydéric Bocquet, David Quéré, Thomas A. Witten and Leticia F. Cugliandolo.

Published 2017 by Oxford University Press.

Chapter Contents

3.1 Introduction

In this set of notes, we will pursue two different themes:

(a) Pinch-off
Very often free-surface singularities are associated with topological transitions, e.g., one piece of material breaking into two, or several pieces being joined into one. Such a transition cannot be smooth, and therefore is associated with a singularity of the underlying equations of motion. Imagine for example a dripping tap (see Fig. 3.1). At the moment of pinch-off, a new structure is born: a drop. We would like to understand the exact form and evolution of the interface near the moment of drop detachment. How is the solution continued across the singularity? Is this continuation unique?

(b) Making small things
Other free-surface singularities are steady, yet produce very small structures on the surface of a liquid. This is best seen in a home experiment: pour olive oil into a glass beaker already filled with oil (see Fig. 3.2). At small speeds of impact the surface is hardly disturbed. On increasing the height of impact, the stream of oil produces a crater which ends in a very sharp cusp, and joins the stream on the other side. Viewed from the side, the crater is visible as a silvery dip. As the height of fall is increased, suddenly a thin sheet of air will shoot out from the tip of the cusp, which is wrapped around the region of impact, and visible from the side as a silvery sliver. Soon the beaker is filled with air bubbles, as

Fig. 3.1 A drop of water about to pinch off. Source: Wikipedia.

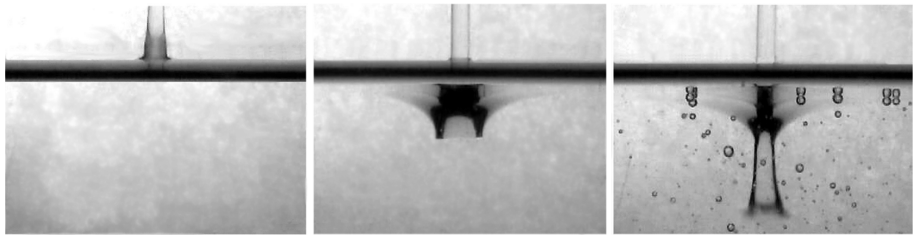

Fig. 3.2 A stream of viscous fluid impacting on a surface of the same fluid. The speed of impact is increasing from left to right. Photos by E. Lorenceau.

the air sheet becomes unstable at its lower end. This is the mechanism by which air is entrained into viscous liquids, for example when beating an egg.
What is interesting about this sequence of events is that it contains a potential mechanism to make small things, without ever fashioning a tool that works on the desired length scale. Instead, we harness the non-linear character of the hydrodynamic equations to focus flow into very small structures.

What are the big ideas at work here?

1. The hydrodynamic equations of motion evolve toward singularities spontaneously, producing very small scales.
2. **Scaling**: the singular evolution is self-similar; this means that the same shapes reappear on smaller and smaller scales.
3. **Universality**: the singularity imposes a unique structure with a limited number of free parameters.

For each case, we will discuss a particularly simple example below, which hopefully will elucidate the general aim.

3.2 Bubble pinch-off in a viscous fluid

We consider an axisymmetric gas bubble (or another low-viscosity liquid), in a viscous liquid. For example, Fig. 3.3 shows a drop of water dripping into a very viscous oil which is slightly lighter than the water. As a result, the drop of water falls, and eventually pinches off.

3.2.1 Equation of motion

Fig. 3.4 shows the flow geometry of a slender axisymmetric bubble in a viscous fluid. We consider the special case that

(i) the outer fluid is sufficiently viscous for inertia to be negligible: we will describe it using Stokes's equation,
(ii) the viscosity of the inner fluid (or gas) is sufficiently small so that it has no dynamical effect at all.

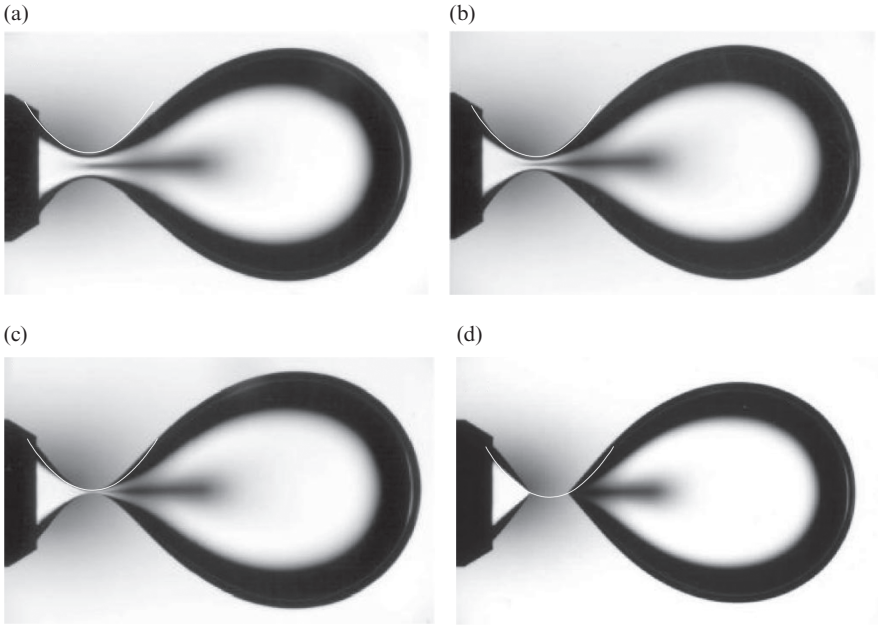

Fig. 3.3 A water drop dripping through silicone oil, whose viscosity is about 10^4 times greater than that of water [2]. (Photo courtesy of S. Nagel and I. Cohen). A parabola is fitted to the first profile (a), and then shifted toward the axis to obtain an optimal fit. In (d), the parabola intersects with the axis to give two separate pieces.

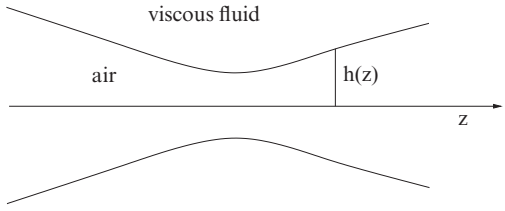

Fig. 3.4 Sketch of a pinching bubble.

In this particular limit, the dynamics are particularly simple [2]. Indeed, from incompressibility we have

$$\nabla \cdot \mathbf{v} = \frac{\partial v_z}{\partial z} + \frac{\partial v_r}{\partial r} + \frac{v_r}{r} = 0.$$

Assuming that the interface is almost flat so that the flow is approximately radial ($\mathbf{v} \approx v_r \mathbf{e}_r$), it follows that

$$v_r = \frac{A(t)}{r}.$$

But since the flow has to move with the interface, we have $v_r(h) = \dot{h}$; in other words,

$$\mathbf{v} = \frac{\dot{h}h}{r}\mathbf{e}_r. \tag{3.1}$$

For a radial flow, the Laplacian of a vector is [8]:

$$\triangle\mathbf{v} = \left(\frac{\partial^2 v_r}{\partial r^2} + \frac{1}{r}\frac{\partial v_r}{\partial r} - \frac{v_r}{r^2}\right)\mathbf{e}_r = 0,$$

so Eq. (3.1) solves the Stokes equation with a constant pressure distribution. At the boundary, the normal stress jump across the interface must balance the Laplace pressure γ/h:

$$\frac{\gamma}{h} = \sigma_{rr} + p_{in} = -\Delta p(t) - 2\eta\frac{\dot{h}}{h},$$

where p_{in} is the pressure in the interior. For $h \to 0$, the pressure jump Δp is negligible, so the equation becomes simply

$$\frac{\partial h}{\partial t} = -\frac{\gamma}{2\eta} = const. \tag{3.2}$$

3.2.2 Pinch-off

After rescaling (the unit of time, for example), Eq. (3.2) becomes

$$\dot{h} = -1. \tag{3.3}$$

Of course this problem can be solved easily: if $h_0(z)$ is the initial condition at time $t = 0$, then the solution of Eq. (3.3) is

$$h(z,t) = h_0(z) - t. \tag{3.4}$$

Thus the initial profile is translated rigidly toward the x-axis; based on an analysis of Eq. (3.4) one could obtain a complete description of the pinch-off process without much ado. However, here we are going to do it the hard way by deploying the machinery of local self-similar analysis using the equation of motion, (3.3). It will turn out that most of the steps we will be going through are very similar to those encountered in more difficult problems involving partial differential equations (only simpler), so hopefully this will be educational.

We want to study the neighborhood of the singular point where h goes to zero. We assume that this occurs at time $t = t_0$, and at $z = z_0$ in space. We will study the limit of the time distance $t' = t_0 - t$ from the singularity going to zero. The spatial distance from the pinch point is denoted by $z' = z - z_0$. To describe the dynamics close to the pinch point, we use the self-similar ansatz

$$h(z',t') = t'^{\alpha}H(\xi), \quad \text{where} \quad \xi = \frac{z}{t'^{\beta}}. \tag{3.5}$$

This corresponds to a scale-invariant dynamics, which lacks any intrinsic length scale. Plugging Eq. (3.5) into the equation of motion (3.3) yields

$$-\alpha t'^{\alpha-1} H + \beta t'^{\alpha-1} \xi H' = -1.$$

To make sure that terms balance in the limit $t' \to 0$ we must have $\alpha = 1$ and we obtain the *similarity equation*

$$H - \beta \xi H' = 1. \tag{3.6}$$

Note that the exponent β, which describes the width of the singularity in space, is as yet undetermined. This situation, in which the scaling is not determined by the intrinsic structure of the equation, is known as "self-similarity of the second kind" [1].

The solution to Eq. (3.6) is

$$H = 1 + a\xi^{1/\beta}, \tag{3.7}$$

where a is a constant of integration. This describes the *inner solution* close to the pinch point. To make sure that this solution is consistent globally, two conditions must be met:

(i) A *matching condition*, which stipulates that at some finite distance Δ from the pinch point the solution is static on the time scale t' of the singular region. This means that the limit

$$\lim_{t' \to 0} h(\Delta, t') = h(\Delta, 0) > 0$$

must be finite, or in other words the singularity only occurs at a point rather than a finite interval. Using the similarity description in Eq. (3.5), it follows that

$$\lim_{\epsilon \to 0} \left[\epsilon H \left(\frac{\Delta}{\epsilon^{\beta/\alpha}} \right) \right]$$

must be finite for Δ both positive and negative. This implies that $H(\xi)$ must satisfy the boundary condition

$$H(\xi) = a_{\pm} \xi^{\alpha/\beta}, \quad \xi \to \pm\infty. \tag{3.8}$$

In our case, from the solution (3.7) we find

$$H \propto \xi^{1/\beta},$$

so Eq. (3.8) is satisfied automatically if $a \neq 0$. Indeed, if a were zero, the drop would have to shrink to zero everywhere in space, which is clearly not consistent with boundary conditions (for example a constant radius at the nozzle).

(ii) A *regularity condition* on $\xi \in \mathbb{R}$, which guarantees that the solution (3.7) does not have any (other) singularities except the pinch-off singularity being described by Eq. (3.5). But this means that $1/\beta$ must be a positive integer; otherwise, Eq. (3.7) would have a singularity for $\xi = 0$. In addition $1/\beta$ must also be even and $a > 0$; otherwise, the denominator would become negative.

In other words, we find a discrete spectrum of exponents

$$\beta_i = \frac{1}{2(i+1)}, i = 0, 1, \ldots. \tag{3.9}$$

The similarity profile is

$$\bar{H}(\xi) = 1 + a\xi^{2(i+1)}, \quad i = 0, 1, 2, \ldots, \tag{3.10}$$

with $a > 0$. The fact that β is determined by a regularity condition is a characteristic property of self-similarity of the second kind. However, we still have an infinite set of possible solutions and the question arises as to which solution will be realized in a particular physical situation. To answer to this question, we will have to look at the *stability* of solutions.

3.2.3 Stability

To study the dynamics we introduce the new time variable $\tau = -\ln t'$, so the solution is represented in the coordinate system (ξ, τ):

$$h(z', t') = t'^{\alpha} H(\xi, \tau). \tag{3.11}$$

Now since $d\tau/dt' = -1/t'$, the equation of motion (3.3) becomes

$$H_\tau = H - \beta\xi H' - 1, \tag{3.12}$$

which we will call the *dynamical system*. The crucial advantage of this description is that any similarity solution $\bar{H}(\xi)$ is a *fixed point* of the dynamical system (3.12). Thus the stability can be studied with the simple exponential ansatz

$$H(\xi, \tau) = \bar{H}(\xi) + \delta e^{\nu\tau} P(\xi), \tag{3.13}$$

where ν is the eigenvalue and P the eigenfunction. If ν is positive, the solution will be driven away from the fixed point.

Inserted into Eq. (3.12), the eigenvalue equation becomes

$$\nu P = P - \beta\xi P' \equiv \mathcal{L}P. \tag{3.14}$$

Again this equation is easy to solve, with the result

$$P = \xi^{(1-\nu)/\beta}.$$

For each β_i there is a discrete sequence of eigenvalues determined by the regularity condition $(1-\nu)/\beta_i = j$, where $j = 0, 1, 2, \ldots$ Thus finally we obtain

$$P = \xi^j, \quad \nu_j^{(i)} = 1 - \frac{j}{2(i+1)}. \tag{3.15}$$

The sequences for the first two similarity solutions are

$$\nu^{(0)} = 1, 1/2, 0, -1/2, \ldots, \quad \text{ground state}$$
$$\nu^{(1)} = 1, 3/4, 1/2, 1/4, 0, -1/4, \ldots, \text{1st excited state.}$$

It thus seems as if *all* similarity solutions were unstable, since they all have positive eigenvalues. Their number increases with the order i of the solution. However, this conclusion is premature; we have overlooked the fact that in our similarity description everything is defined with respect to z_0 and t_0, whose actual values should not matter. However, if the initial condition is perturbed (with some small amplitude ϵ, for instance), the space and time coordinates of pinch-off will change as well: $z_0 = z_0(\epsilon)$, $t_0 = t_0(\epsilon)$. Thus no break-up will in fact occur at the unperturbed coordinates $z_0(0)$ and $t_0(0)$, which can only mean that the dynamics has diverged from the self-similar dynamics. Instead, to see singular behavior, the origin (z_0, t_0) has to be adjusted to remain at the singular point.

This can be investigated more formally by observing that for any Δ,

$$h^{(\Delta)} = t'^{\alpha} \bar{H}\left(\frac{z' + \Delta}{t'^{\beta}}\right) \equiv t'^{\alpha} H^{(\Delta)}(\xi, \tau)$$

is a similarity solution of Eq. (3.3). If $h^{(\Delta)}$ is expanded in Δ, we find

$$H^{(\Delta)}(\xi, \tau) = \bar{H}(\xi) + \Delta t'^{-\beta} \bar{H}_\xi + O(\Delta^2) \equiv \bar{H}(\xi) + \Delta e^{\beta\tau} \bar{H}_\xi. \tag{3.16}$$

This means that the term linear in Δ must be a solution of Eq. (3.14) with eigenvalue $\nu = \beta$ and eigenfunction

$$\bar{H}_\xi = 2(i+1) a \xi^{2i+1} = 2(i+1) a P_{2i+1}^{(i)}(\xi).$$

An almost identical calculation, but perturbing the time coordinate instead of the spatial coordinate, yields another positive eigenvalue of $\nu = 1$. The vanishing eigenvalue of the ground state comes from shifting a, which corresponds to the arbitrariness of the axial scale. The corresponding eigenfunction is

$$\frac{\partial \bar{H}}{\partial a} = \xi^{2(i+1)} \equiv P_{2(i+1)}^{(i)}(\xi).$$

Inspection of the ground-state sequence of eigenvalues for the ground state shows that this accounts for all the non-negative eigenvalues. All other eigenvalues are negative, and so the ground-state solution is *stable*. By contrast, the eigenvalue series $\nu^{(1)}$, apart from the values $1, 1/4$, and 0, still contains $3/4$ and $1/2$ as positive eigenvalues. As a result this solution (and even more so those of higher order), is unstable.

In conclusion, there is a unique similarity solution H_b which is stable, describing the pinch-off *before* the singularity:

$$h(z', t') = t' H_b(\xi), \quad H_b(\xi) = 1 + a\xi^2. \tag{3.17}$$

Geometrically, this corresponds to a parabola which is shifted at a constant rate in the direction of the axis (see Fig. 3.3). By fitting the parabola at some initial time, good agreement is achieved in the pinch region. Indeed, the stability calculation provides us with information on how the self-similar behavior in Eq. (3.17) is *approached*, as other possible similarity solutions decay away.

Summing up all eigensolutions of the linear problem (3.14), we obtain

$$h(z', t') = t' \left\{ 1 + a\xi^2 + \sum_{j=0}^{\infty} a_j t'^{j/2-1} \xi^j \right\}.$$

However, we have seen that by changing the values of z_0, t_0, and a, the first three eigenfunctions are generated. Thus by adjusting their values suitably, the first three terms in the sum can be made to vanish and we obtain

$$h(z', t') = t' \left\{ 1 + a\xi^2 + \sum_{j=3}^{\infty} a_j t'^{j/2-1} \xi^j \right\}, \tag{3.18}$$

where the correction is seen to vanish in the limit $t' \to 0$. Corrections are controlled by the smallest (by absolute value) scaling exponent, which is $1/2$ in this case. In critical phenomena, this would be called the Wegner exponent [12].

3.2.4 Continuation

In Fig. 3.5 we summarize what we have done so far and indicate how to go beyond. On the left we start from a smooth profile $h_0(z)$, which generically will have a single quadratic minimum at z_{min} where the radius is h_{min}. According to Eq. (3.4), this profile is to be shifted rigidly toward the z-axis until it touches. The neighborhood of the point z_{min} is the singularity we have investigated so far. If we continue beyond the singular time $t_0 = h_{min}$ the profile intersects the z-axis.

While parts with $h(z, t)$ negative clearly make no sense in terms of the physical interpretation as a radius, Eq. (3.4) can still be interpreted as the *continuation* of Eq. (3.4) across the singularity. Namely, the solution after the singularity can be defined as the parts of Eq. (3.4) for which $h(x, t)$ is positive (see Fig. 3.5 (right)). At the bottom, we have drawn a cross section through the drop only for the pieces for which h is positive. After the singularity the domain is *multiply* defined, as a result of the solution having undergone a topological transition. In the absence of an exact solution like Eq. (3.4) there are two different ways to deal with the fact that the drop has split up into different pieces, as illustrated in Fig. 3.6. In the first method, we only consider places where $h > 0$, and develop an equation of motion for the boundaries of the drop as well as for the drop profile itself. In the second method (bottom), we *regularize*

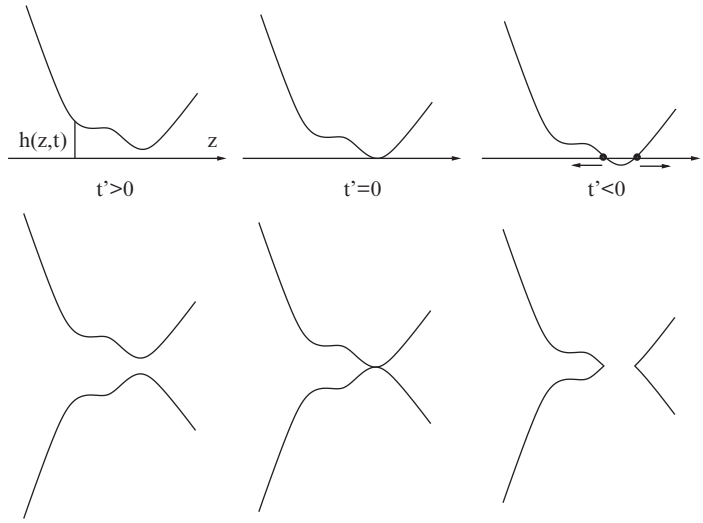

Fig. 3.5 A simple model for the experimental sequence of drop pinch-off shown in Fig. 3.3. At $t' = 0$, the radius goes to zero, for $t' < 0$, the drop consists of two pieces (bottom row). In the top row it is shown how the dynamics are generated by a simple *shift* of the profile at a constant rate. After the profile has intersected with the x-axis two fluid threads retract on either side of the pinch point.

the dynamics so that it is defined everywhere in space, but where the inside and the outside of the drop represent two different "phases," from which the position of the drop can be reconstructed. We now describe both methods in turn.

3.2.4.1 Sharp interface description

The dynamics after the singularity is formulated in the "physical" domain alone, and the boundary between a drop and its exterior is represented by a sharp interface. In that case, apart from the dynamics in the interior of the drop itself one needs a separate equation for the motion of the interface position. In the context of numerical methods one speaks of "front tracking" [7]. Since the condition for a boundary point z_b is $h_0(z_b) = t$ an equation of motion for the boundary point is found by differentiating with respect to time: $\dot{z}_b h'(z_b, t) = 1$, where the prime denotes the derivative with respect to the spatial argument. Considering for simplicity two boundary points only (see Fig. 3.5), we arrive at the following post-break-up dynamics:

$$\frac{\partial h}{\partial t} = -1, \quad z < z_b^{(1)} \text{ or } \quad z > z_b^{(2)} \tag{3.19}$$

$$\frac{\partial z_b^{(i)}}{\partial t} = \frac{1}{h'(z_b^{(i)}, t)}, \quad i = 1, 2. \tag{3.20}$$

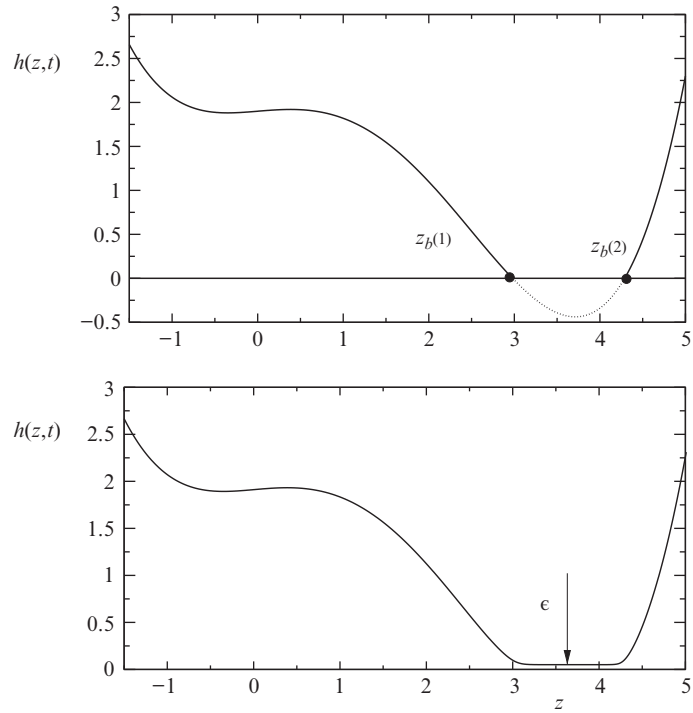

Fig. 3.6 A profile after the singularity, as described by Eq. (3.19) (top). The solution is defined for $z < z_b^{(1)}$ and $z > z_b^{(2)}$. At the bottom is a solution of Eq. (3.21) with the same boundary conditions and $\epsilon = 0.05$. This solution is defined for all z, and tends toward the continuation in the limit $\epsilon \to 0$.

After break-up, the equation of motion (3.19) has to be solved in two separate domains, while the boundary points are tracked using Eq. (3.20).

3.2.4.2 Diffuse interface description

The split into two or more domains brings with it the complication of having to solve several separate problems at the same time, and to trace the boundaries of each domain. To avoid this complication and to solve the problem in a single domain, one can look at the same phenomenon using a *regularized* version of the equation of motion (3.3) which does not exhibit "singularities" $h \to 0$. For example, consider

$$\frac{\partial h}{\partial t} = -1 + \frac{\epsilon}{h(z,t)}, \quad h(z,0) = h_0(z). \tag{3.21}$$

Now the "repulsive" term ϵ/h ensures that $h(z,t)$ never goes through zero, but rather forms a thin "thread" of thickness ϵ.

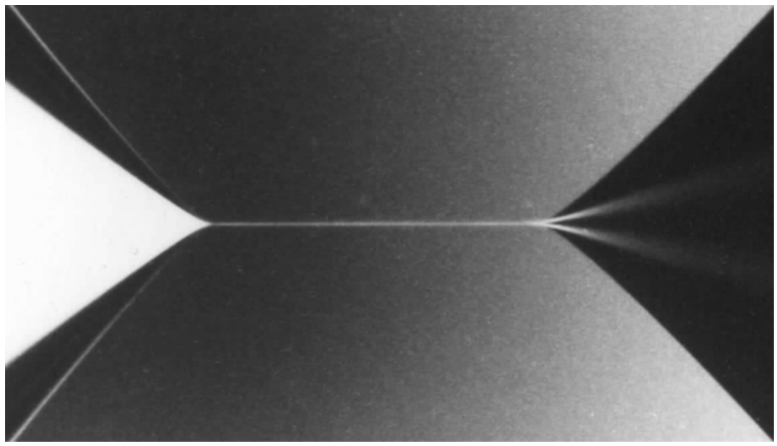

Fig. 3.7 A thin thread of water remains between the two pieces. (Photo courtesy of S. Nagel and I. Cohen.)

As illustrated in Fig. 3.6, in the limit of small ϵ the regularized model in Eq. (3.21) describes essentially the same problem as the continuation in Eq. (3.19). Outside the two domains of this solution, a thin "thread" remains whose thickness is ϵ. In fact, such a thin thread (about 8 μm) is observed in the actual experiment [2] (see Fig. 3.7), owing to the presence of the inner fluid. The viscous stresses in the thin thread delay further thinning. However, we do not claim that Eq. (3.21) is a good model of this effect; here we are merely interested in illustrating the principle of regularization.

What is the structure of the continued solution shortly after "pinch-off" (defined by the original dynamics in Eq. (3.3))? This question can be answered by an asymptotic analysis of Eq. (3.21). Here we cheat a little, and simply use the exact solution of Eq. (3.21). Namely,

$$dt = \frac{h}{\epsilon - h} dh,$$

and so

$$t_0(z) - t = h + \epsilon \ln(h - \epsilon). \tag{3.22}$$

Clearly, at places where the left-hand side is negative (which occurs after the singularity of the unregularized equation) we must have $h \to \epsilon$.

The (extrapolated) break-up time is shifted by an amount ϵ:

$$t_0(0) \approx h_0(0) + \epsilon \ln(h_0(0)),$$

where $h_0(0)$ is the minimum height at the initial time $t = 0$. More generally, since Eq. (3.22) must match onto the solution Eq. (3.18) for $h \gg \epsilon$ we have

$$t_0(z) - t \approx t'(1 + a\xi^2) + \epsilon \ln(h_0),$$

which determines $t_0(z)$. Inserting this back into Eq. (3.22), we obtain

$$t'(1+a\xi^2) = h + \epsilon \ln \frac{h-\epsilon}{h_0}.$$

We solve this for $h \to \epsilon$, where we expect the solution to be of the form $h \approx \epsilon + \epsilon^2 \delta(x,t)$. Then

$$t'(1+a\xi^2) = \epsilon + \epsilon^2\delta + \epsilon \ln \frac{\epsilon^2\delta}{h_0}$$

and neglecting terms quadratic in ϵ,

$$h = \epsilon + \frac{h_0}{e\epsilon^2} \exp\left\{\frac{t' + az'^2}{\epsilon}\right\}, \tag{3.23}$$

valid for $t' < 0$ and $\epsilon \to 0$. From Eq. (3.23) one reads off the following features: the length of the filament of thickness ϵ is determined by the requirement that the expression in the exponent remains negative. The boundary of this region is determined by $t' + az_{tip}^2 = 0$, or

$$z_{tip} = \pm\sqrt{\frac{-t'}{a}}. \tag{3.24}$$

A straightforward analysis shows that the width of the transition region at the edge of the thread (the interface thickness) is

$$\delta_b \approx \frac{\epsilon}{az'_{tip}}, \tag{3.25}$$

which goes to zero for $\epsilon \to 0$. This means the diffuse interface description approaches the dynamics described by Eqs (3.19) and (3.20) in a pointwise fashion.

3.2.4.3 Similarity description of continuation

Above we have addressed the problem of continuation in two different ways: first geometrically and then by regularizing the dynamics. However, a simple geometrical formulation is not always available to us, and the regularized dynamics is often complicated and not amenable to analytical treatment. It is therefore very useful to look at a third way of treating the problem, namely using the similarity description. So far we have used it to describe the dynamics before the singularity, and the solution for $t' > 0$ is described by Eq. (3.17).

We look for similarity solutions *after* breakup ($t' < 0$) of the form:

$$h_a = |t'| H_a(\xi), \quad \xi = z/|t'|^{1/2}, \tag{3.26}$$

so that $|t'|$ remains positive. Note that $|t'| = t - t_0$, so the time derivatives change sign, and we obtain a new similarity solution

$$H - \xi H'/2 = -1, \tag{3.27}$$

with solution

$$H_a = -1 + \bar{a}\xi^{1/\beta}; \tag{3.28}$$

both $\bar{a}$ and the exponent β are undetermined at this point.

The values of $\bar{a}$ and β must be found by matching to the prebreak-up solution. Namely, at a finite (but arbitrarily small) distance Δ from the pinch point, the solution must remain the same as one passes through the singularity. Thus one obtains the matching condition

$$\lim_{t'\to 0} h_b(\Delta, t) = \lim_{t'\to 0} h_a(\Delta, t). \tag{3.29}$$

Inserting the similarity solutions (3.17) and (3.28) into Eq. (3.29), we find that

$$1 + a\frac{\Delta^2}{|t'|} \sim -1 + \bar{a}\left(\frac{\Delta}{|t'|^{1/2}}\right)^{1/\beta}$$

in the limit $t' \to 0$. Clearly, this can only be satisfied if $\beta = 1/2$ and $\bar{a} = a$. In other words, the matching procedure uniquely determines the post-break-up solution:

$$H_a = -1 + a\xi^2. \tag{3.30}$$

There are two branches of solutions to Eq. (3.30), corresponding to the two receding threads on either side of the pinch point. The tips of the threads are located at the point $h = 0$; that is, at $\xi_\pm = \pm 1/\sqrt{a}$. In terms of the physical variables this means that the tip positions are at

$$z_{tip} = \pm|t'|^{1/2}/\sqrt{a} \tag{3.31}$$

in agreement with Eq. (3.24), obtained from the diffuse interface description in the limit $\epsilon \to 0$. Thus just after the singularity the two tips recede at a speed

$$\dot{z}_{tip} = \pm\frac{1}{2\sqrt{a}}|t'|^{-1/2}, \tag{3.32}$$

which is diverging as the singularity is approached.

In conclusion, we find a unique continuation to a post-break-up solution, whose parameters are determined by the dynamics before break-up. Close to the tip, the assumption of a slender filament evidently breaks down. For example, a thin thread remains (c. Fig. 3.7), which will alter the neighborhood of the tip. However, this should not alter the asymptotics away from the tip, as the large-scale dynamics are determined uniquely.

Geometrically, the solution (3.30) corresponds to a parabola which intersects with the z-axis. A comparison to Fig. 3.3 (d) shows a satisfactory agreement of the experiment with this result. It appears that the two pieces are a little closer together than expected. A possible explanation is that the remaining thread pulls the two pieces together, an effect not accounted for by the theory.

3.3 Cusps on the surface of a viscous fluid

Singularities that form on the surface of a viscous liquid are very common, as we saw for example in Fig. 3.2. Another prototypical experiment is shown in Fig. 3.8. Two counter-rotating cylinders are mounted beneath the surface of a viscous liquid. In the region of converging flow between the two rollers the surface becomes strongly deformed and appears to end in a cusp, that is, a point where the two tangents to the curve become parallel. At even higher rates of rotation (with a threshold value to be determined) the cusp undergoes a bifurcation and a sheet of air shoots out from the cusp and into the fluid.

However, the cusp-forming mechanism that leads to strong deformations of the interface applies more generally, and is not restricted to quasi two-dimensional experiments such as the one shown above. For example, imagine beating an egg to produce a foam. The object is to entrain as much air as possible into the liquid. This happens because cusp singularities first form on the free surface, which subsequently act as seeds for air to enter the liquid. Note that if the free surface were to remain smooth it would be very difficult for any other phase to enter the liquid. An interesting question is to determine the nature of singularities in a very complicated (random) flow field, such as that produced by the egg beater.

3.3.1 Cusp structure

We will see in subsection 3.3.2 that the tip is actually rounded on a small scale, but for now we treat it as a perfect cusp around which we solve the viscous flow equations. This is difficult because as yet we do not know the precise shape of the surface. However, Fig. 3.9 suggests a simplification: viewed from a large scale, we have to solve the flow

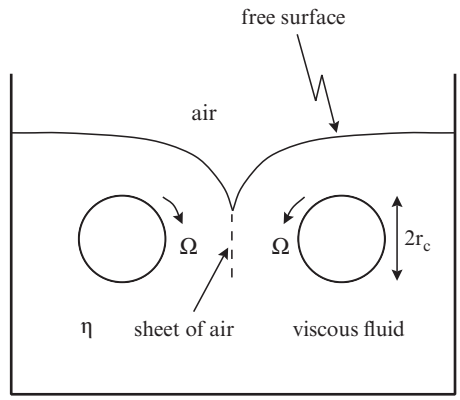

Fig. 3.8 Sketch of an experiment conceived by Joseph et al. [6], and perfected by Lorenceau et al. [10]. Two rollers are counter-rotating below a free surface inside a viscous liquid. On the line of symmetry, a sharp cusp is formed between them on the free surface. At even higher rates of rotation, the cusp tip "opens" and a sheet of air shoots out into the liquid. As a result, air is entrained into the liquid.

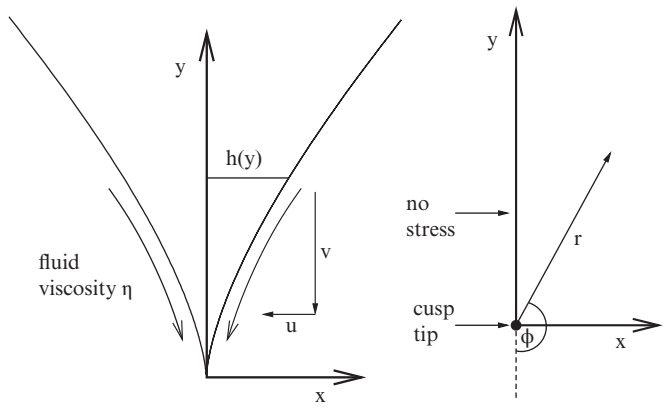

Fig. 3.9 A cusp singularity in a viscous fluid and the flow around the free surface (left). On the right, a coarse-grained version of the same problem: flow in a slit plane. The boundary condition on the upper half of the y-axis is one of no stress.

equations in a plane with a cut, which represents the cusp. Note that the geometry resembles that of a *crack* in an elastic medium.

Solving Stokes' equation in a plane is equivalent to solving the biharmonic equation for the *stream function* ψ, that is

$$\triangle^2 \psi = 0. \tag{3.33}$$

The problem is solved most conveniently in polar coordinates, with the origin at the tip of the cusp. Given ψ, the velocity field is calculated as

$$u_r = \frac{1}{r}\frac{\partial \psi}{\partial \phi}, \quad u_\phi = -\frac{\partial \psi}{\partial r}.$$

The idealized problem is *scale invariant*, and therefore we are looking for *similarity solutions* of the form

$$\psi = r^\lambda f(\phi). \tag{3.34}$$

Inserting Eq. (3.34) into Eq. (3.33), we find symmetric solutions of the form

$$f = A\sin(\lambda\phi) + C\sin((\lambda - 2)\phi).$$

In Fig. 3.9 we have chosen for the cusp to lie along $\phi = \pi$, so that Eq. (3.34) obeys the boundary condition $u_\phi = 0$ on the line of symmetry $\phi = 0$ automatically. By contrast, the velocity perpendicular to the face of the cut is not zero. Indeed, in view of the "near field" picture Fig. 3.9 (left), our goal is to calculate the velocity field u_ϕ pointing inwards toward the cusp, from which we will compute the shape of the free surface.

Along the cut, i.e., for $\phi = \pi$, we impose boundary conditions of zero shear and zero normal stress:

$$\mathbf{n}\boldsymbol{\sigma}\mathbf{t} = \sigma_{r\phi} = 0, \quad \mathbf{n}\boldsymbol{\sigma}\mathbf{n} = \sigma_{\phi\phi} = 0,$$

which in polar coordinates reads as

$$\sigma_{r\phi} = \eta\left(\frac{1}{r}\frac{\partial u_r}{\partial \phi} + \frac{\partial u_\phi}{\partial r} - \frac{u_\phi}{r}\right) = 0 \text{ and } \quad \sigma_{\phi\phi} = 2\eta\left(\frac{1}{r}\frac{\partial u_\phi}{\partial \phi} + \frac{u_r}{r}\right) - p = 0, \quad (3.35)$$

respectively. The pressure can be eliminated from Eq. (3.35) by taking the r-derivative of the second equation and using the r-component of the Stokes equation:

$$\frac{\partial p}{\partial r} = \eta\left(\frac{\partial^2 u_r}{\partial r^2} + \frac{1}{r^2}\frac{\partial^2 u_r}{\partial \phi^2} + \frac{1}{r}\frac{\partial u_r}{\partial r} - \frac{2}{r^2}\frac{\partial u_\phi}{\partial \phi} - \frac{u_r}{r^2}\right),$$

so in terms of the stream function, Eq. (3.35) becomes

$$\frac{1}{r^2}\frac{\partial^2 \psi}{\partial \phi^2} + \frac{1}{r}\frac{\partial \psi}{\partial r} - \frac{\partial^2 \psi}{\partial r^2} = 0, \quad \frac{3}{r}\frac{\partial^3 \psi}{\partial r^2 \partial \phi} + \frac{1}{r^3}\frac{\partial^3 \psi}{\partial \phi^3} - \frac{3}{r^2}\frac{\partial^2 \psi}{\partial r \partial \phi} + \frac{4}{r^3}\frac{\partial \psi}{\partial \phi} = 0. \quad (3.36)$$

Evaluating Eq. (3.36) at $\phi = \pi$, one finds the two conditions

$$(\lambda - 1)\left[\lambda A + (\lambda - 2)C\right]\sin \lambda\pi = 0 \text{ and } \lambda(\lambda - 1)(\lambda - 2)\left[A + C\right]\cos \lambda\pi = 0. \quad (3.37)$$

Solutions to Eq. (3.37) either have to obey $\sin \lambda\pi = 0$ or $\cos \lambda\pi = 0$, while the other equation yields a relation between the two amplitudes A and C. This means there is an infinite sequence of solutions $\lambda = \pm i/2$ where i is an integer. But since the velocity is a derivative of ψ, the velocity will diverge if $\lambda < 1$. Thus the first possible solution is $\lambda = 1$, which leads to the solution

$$\psi = (A - C) r \sin \phi.$$

This is the velocity of a uniform velocity v in the y-direction, streaming past the cusp; let us take this stream to be $v = -U$. The next possibility is $\lambda = 3/2$, which solves the second equation in (3.37) and yields $C = 3A$ from the first equation. Thus the total solution, from a superposition of the first two, is

$$\psi = Ur \sin \phi - 4Ar^{3/2} \sin^3 \frac{\phi}{2} \quad (3.38)$$

valid near the tip. Evaluating this along the crack $\phi = \pi$ the Cartesian components of the velocity field are

$$u = -u_\phi = \frac{\partial \psi}{\partial r} = -6Ay^{1/2}, \quad v = -U. \quad (3.39)$$

Now we return to the near-field description, illustrated in Fig. 3.8 (left). We use the flow field (3.39), observing that a stationary free surface will be a streamline of the flow. Therefore, we have

$$\frac{\partial h}{\partial y} = \frac{u}{v} \approx \frac{6A}{U} y^{1/2}.$$

Integrating this equation, we finally arrive at

$$h \approx \frac{4A}{U} y^{3/2}. \tag{3.40}$$

We see that the cusp is characterized by a 3/2 similarity index. In particular this occurs near the tip $h \ll y$ so that the cusp indeed becomes narrow, justifying the approximation as a slit of vanishing thickness.

3.3.2 A generic picture

The above calculation suggests that the power law index is very specific to the equations of viscous flow. But what happens for other cusps? Take for example a cycloid, i.e., the trajectory of a point on the boundary of a unit circle, rolling on a line (see Fig. 3.10). As the point hits the line it experiences a sudden reversal in its direction of motion and the trajectory must have a cusp, as shown in the middle of Fig. 3.10. What is the structure of this cusp? To answer this question, consider the trajectory of a point which is a distance $\epsilon > 0$ inside the circle. Then the reversal is no longer so sudden, and one finds the rounded cusp shown on the left. If on the other hand the point lies a distance $-\epsilon$ *outside* of the circle, the curve self-intersects, as shown on the right.

From elementary kinematic considerations one finds that for general ϵ the curve is described by

$$x = s - (1-\epsilon)\sin s, \quad y = 1 - (1-\epsilon)\cos s, \tag{3.41}$$

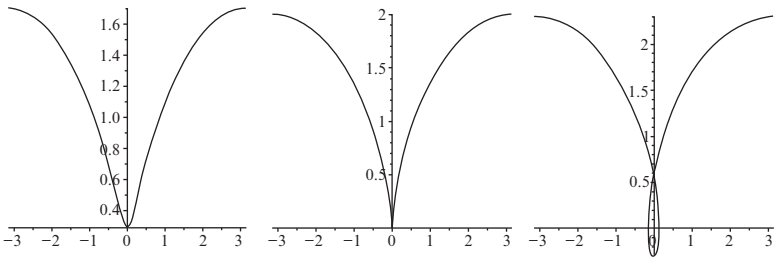

Fig. 3.10 In the middle, we show the singular curve of a cycloid, i.e., the line traced out by a point on the boundary of a rolling circle. On the left, the position of the curve is moved a distance $\epsilon > 0$ toward the center of circle, yielding a smooth curve. For $\epsilon < 0$, i.e., a point outside the circle, the curve self-intersects.

where s parameterizes the curve. As ϵ is varied smoothly from negative to positive, the curve transforms from a self-intersecting shape to an open curve, with a cusp forming the moment the loop is opened. Instead of analyzing this particular case we ask for the structure of a family of smooth curves $\mathbf{x}(s,\epsilon)$ which have a critical point $\dfrac{\partial \mathbf{x}}{\partial s} = 0$ for $\epsilon = 0$.

To analyze this situation we expand the coordinates of the curve in s, which parameterizes the curve assuming that the critical point occurs for $s = 0$. Then to leading order, we obtain

$$x = x_0 + a_1 s, \quad y = y_0 + a_2 s.$$

The parameters x_0 and y_0 can be eliminated by a translation and $a_2 = 0$ after a suitable rotation. For a critical point to occur at $s = 0$ a_1 must also vanish. Otherwise, the curve would be a straight line locally. Thus we put $a_1 = \epsilon$ where $\epsilon = 0$ is the critical point. For the curve not to become degenerate, we must expand to higher order. Thus to leading order $y = s^2/2$, normalizing the prefactor to $1/2$ by rescaling s. In the other coordinate, we must go to higher order, since the choice $x = \epsilon s + bs^2$ would once more result in a degenerate curve at the critical point $\epsilon = 0$. Thus we obtain a third-order polynomial $x = \epsilon s + bs^2/2 + as^3/3$. Using a shift in s and another rotation, the coefficient b can be eliminated so we finally obtain the universal form:

$$x = \epsilon s + as^3/3, \quad y = s^2/2. \tag{3.42}$$

At the critical point $\epsilon = 0$ this gives $x \propto y^{3/2}$, exactly as Eq. (3.40) obtained previously from quite a laborious calculation. However, this calculation only applies to the critical case $\epsilon = 0$, whereas Eq. (3.42) also describes cusps which are rounded at the tip whose curvature at the apex is $\kappa = \epsilon^{-1}$. With ϵ as the scaling parameter, Eq. (3.42) has the universal similarity form

$$\begin{aligned} x = \epsilon^{3/2} X_c(\sigma), \quad y = \epsilon Y_c(\sigma), \\ X_c = \pm\sigma + a\sigma^3/3, \quad Y_c = \sigma^2/2, \end{aligned} \tag{3.43}$$

with the similarity variable $\sigma = s/\epsilon^{1/2}$. The + sign corresponds to the open curve (see Fig. 3.10 (left)), the − sign to a self-intersecting curve (see Fig. 3.10 (right)).

A local analysis of the generalized cycloid curve (3.41) of course leads to the same family as Eq. (3.42) with self-intersecting curves for $\epsilon < 0$. However, is there any connection to the original fluid mechanics problem shown in Fig. 3.8? An ingenious calculation by Jeong and Moffatt [5], based on an exact solution of the Stokes equation *including* surface tension, shows that this is indeed the case: it yields precisely the similarity form (3.43) of the tip! The Jeong–Moffatt solution is based on a particular flow geometry, where the two cylinders shown in Fig. 3.8 are replaced by a single vortex dipole. However, the generic result in Eq. (3.42) suggests that the cusp structure should be independent of any particular flow geometry. What Eq. (3.42) cannot predict is the actual value of the radius of curvature r of the cusp, which is proportional to ϵ. Instead of reproducing the full calculation [5] which is quite intricate, we merely give a scaling

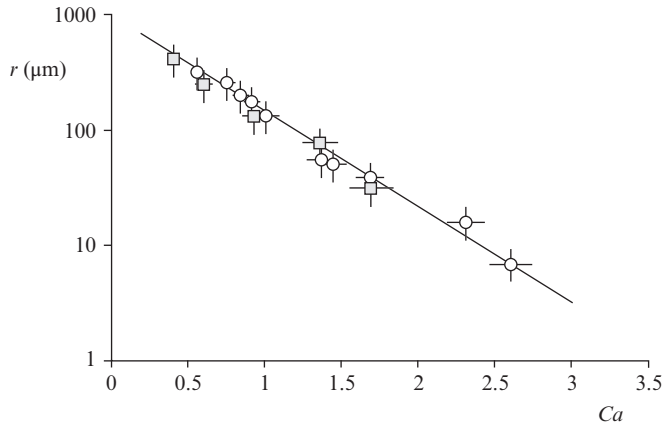

Fig. 3.11 The radius of curvature r of a viscous cusp as function of the capillary number Ca. Lorenceau, E., Restagno, F., and Quere, D. (2003). Fracture of a viscous liquid. *Phys. Rev. Lett.*, 90, 184501.

argument which explains the *exponential* dependence on surface tension. Namely, the effect of surface tension is to generate a point force of strength 2γ (the two sides of the cusp pulling with force γ per unit length in the y-direction) at a distance r inside the cusp. This corresponds to the force being smeared out over the size r of the cusp. At the tip this generates an upward velocity $-2\gamma/(4\pi\eta)\ln r$ which is the velocity generated at a distance r from a point force. For the tip to be stationary, the upward velocity has to be compensated by the downward-sweeping velocity U leading to

$$r \propto e^{-2\pi Ca}, \tag{3.44}$$

where the capillary number is $Ca = \eta U/\gamma$. This exponential relationship (the size of the cusp goes to zero very rapidly with capillary number) is confirmed experimentally in Fig. 3.11.

3.3.3 Entrainment

We now turn to the phenomenon shown in Fig. 3.2. If the capillary number is increased further (for example the speed of the jet impacting the liquid pool is increased, or the rollers in Fig. 3.8 increase their speed of rotation) the cusp undergoes a bifurcation and a thin sheet of air shoots out from the tip of the cusp (5, 10; see also Fig. 3.8). The idea is that the external fluid (often air) is dragged into the cusp and pushes it open. A simplified calculation, which we present now, proceeds in three steps:

i. Calculate the pressure generated by the external fluid inside the cusp.
ii. Calculate the flow modification produced by the external load on the cusp faces.
iii. Calculate the modified interface.

3.3.3.1 Pressure inside the cusp

According to Eq. (3.43), expressed in Cartesian coordinates, the cusp can be written in the similarity form

$$h(y) = \kappa^{-3/4} H(y\kappa^{1/2}) \tag{3.45}$$

where κ is the curvature at the cusp tip and

$$H(\xi) = \sqrt{a\xi}(\xi + \sqrt{2/a})$$

is a universal similarity function. All lengths have been made dimensionless by an appropriate length scale, for example the distance between the rollers in Fig. 3.8. The parameter a is simply a reminder of this arbitrariness in the choice of reference scale; it can be scaled to unity by an appropriate choice of reference scale. The crucial feature of Eq. (3.45) is that the profile is slender ($h' \ll 1$) except of course at the tip itself.

Thus the flow of air inside the cusp can be described using Reynolds' lubrication idea: the flow field is expanded in the x-direction (normal to the cusp walls):

$$v = a_0(y) + a_2(y)x^2 + \dots$$

We assume that the viscosity of the interior fluid is smaller by a factor λ relative to that of the outer fluid (the viscous liquid). The flow field itself is predominantly in the direction of the cusp (y-direction); we only need to consider the y-component of Stokes's equation, $\partial_y p = \lambda\eta\triangle v$. Since the channel is narrow gradients in the transverse direction are greater than those in the downstream direction, and so $\triangle v \approx \partial_x^2 v$. Thus we obtain $p'(y) = 2\lambda\eta a_2$ where the pressure can be considered a function of y only.

Since the channel is closed at the cusp tip the total flux must vanish and we have

$$0 = \int_0^h v dx = h a_0 + \frac{a_2}{3} h^3,$$

or $a_0 = -a_2 h^2/3$. As before, we consider a constant stream of liquid $-U$ at the exterior of the cusp. So owing to the no-slip boundary condition we have $-U = v(h) = 2a_2 h^2/3$, and finally

$$p' = -3\lambda\eta \frac{U}{h^2}. \tag{3.46}$$

Thus our first result shows that the pressure increases strongly as the cusp becomes narrower. It is this pressure increase which keeps two moving mechanical parts from touching, which was the original application of lubrication theory. We should also mention that the assumption of a *constant* external streaming is not strictly correct [3], but rather that there is a slow logarithmic variation. Although we can still use Eq. (3.46) in this case we will disregard this feature in the interest of simplicity.

3.3.3.2 The modified velocity field

Now we calculate how the velocity field in the exterior of the cusp is modified by the presence of the lubrication pressure in Eq. (3.46). To that end, we come back to the slit geometry shown in Fig. 3.9 (right). However, instead of the stress-free homogeneous problem considered so far (which contributes the base flow) we now consider a normal stress $\mathbf{n}\boldsymbol{\sigma} = p\mathbf{n}$ on the face of the cusp where p is the lubrication pressure. As illustrated in Fig. 3.12 this leads to a perturbation to the velocity in the x-direction, away from the cusp. This inhomogeneous problem can be solved by using complex potential theory [11]. The result is

$$u^{(\lambda)}(y) = \frac{1}{\eta}\int_0^\infty p(y')m(y'/y)dy', \tag{3.47}$$
$$m(x) = (1/2\pi)\ln((1+\sqrt{x})/(1-\sqrt{x})),$$

corresponding to an integral over the pressure distribution over the cusp.

3.3.3.3 The modified interface

Now the x-component of the velocity is made up of two contributions: the unperturbed velocity field $u^{(0)}$ and $u^{(\lambda)}$ produced by the lubrication pressure. Since the free surface is a streamline of the flow, we have

$$h' = -(u^{(0)} + u^{(\lambda)})/U. \tag{3.48}$$

Qualitatively, the cusp becomes unstable because $u^{(0)}$ and $u^{(\lambda)}$ have opposite signs (see Fig. 3.12): Namely, as p increases, the x component of the velocity field decreases, making the gap narrower. But as a result, p increases even more, eventually leading to a bifurcation.

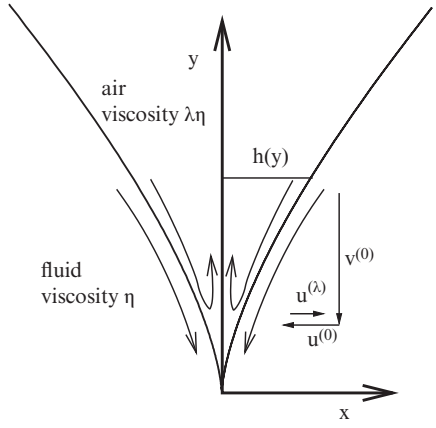

Fig. 3.12 A schematic of the flow inside and outside of the cusp.

This mechanism is best analyzed by recasting everything in the scaling variables of Eq. (3.45), which implies that the x-scale is $\kappa^{-3/4}$ and the y-scale $\kappa^{-1/2}$. First, from Eq. (3.48), $u^{(0)}$ must scale like $\kappa^{-3/4}\kappa^{1/2} = \kappa^{-1/4}$. From Eq. (3.46) p_{lub} is estimated as $p_{lub} \sim \lambda\kappa$, and thus $u^{(\lambda)} \sim \lambda\kappa^{1/2}$ from integrating once. The two opposing velocities become comparable at some critical value of the parameter $s = \lambda\kappa^{3/4}$.

Using this scaling, in terms of the similarity variable $\xi = y\kappa^{1/2}$ we have

$$h(y) = \kappa^{-3/4}\left(H(\xi) + H_c(\xi)\right),$$

where $H_c' = -\kappa^{1/4}u^{(\lambda)}/U$ is the correction to the profile. If we put $p = \lambda\kappa P(\xi)$ we obtain

$$P' = -\frac{3\eta U}{(H + H_c)^2}$$

from Eq. (3.46). Note that the capillary pressure at the cusp tip is of order κ, so a typical lubrication pressure is smaller by a factor of $\lambda \ll 1$. Thus the tip region remains unchanged during the bifurcation, which is due to the pressure on the flanks of the cusp alone. Transforming Eq. (3.47) into similarity variables, we obtain

$$u^{(\lambda)} = \frac{\lambda\kappa^{1/2}}{\eta}\int_0^\infty P(\zeta)m(\zeta/\xi)d\zeta = -\frac{\lambda\kappa^{1/2}}{\eta}\xi\int_0^\infty P'(\zeta)M(\zeta/\xi)d\zeta$$

where $M'(x) = m(x)$, integrating by parts in the second step. Now we finally have

$$H_c'(\xi) = -3s\xi\int_0^\infty \frac{M(\zeta/\xi)}{\left[H(\zeta) + H_c(\zeta)\right]^2}d\zeta, \tag{3.49}$$

which is the equation controlling the stability of the cusp.

We will show that there is a critical value s_c of s above which Eq. (3.49) has no more solutions. But this means that

$$\kappa_c = s_c^{4/3}\lambda^{-4/3}, \tag{3.50}$$

i.e., the cusp curvature at which the transition occurs increases as the viscosity ration becomes smaller. Instead of solving Eq. (3.49) numerically, we will now present a simplified treatment which permits us to calculate the bifurcation analytically. The idea is to pretend that H_c can be written as $H_c \approx c\xi^{3/2}$, where c is to be determined. Then we find that

$$(H + H_c)^2 = \left(\sqrt{a} - c\right)^2\xi\left(\xi + \frac{\sqrt{2}}{\sqrt{a} - c}\right)^2.$$

In other words, the form of the profile remains unchanged; only the parameter a has shifted.

To be able to close Eq. (3.49) we pretend that we can replace $M(x)$ by its asymptotic form for large arguments: $M(x) \approx 2x^{1/2}/\pi$. Then Eq. (3.49) turns into

$$\frac{3c}{2}\xi^{1/2} = \frac{6s}{\pi}\xi^{1/2}\int_0^\infty \frac{\zeta^{1/2}d\zeta}{(H+H_c)^2} = 6s\xi^{1/2}\frac{2^{1/4}}{\sqrt{\sqrt{a}-c}}.$$

In other words, we obtain the equation

$$c = \frac{2^{1/4}s}{\sqrt{\sqrt{a}-c}} \equiv f(c). \tag{3.51}$$

The way in which Eq. (3.51) leads to a bifurcation is illustrated in Fig. 3.13. On the left, we plot $f(c)$ and c versus c—that is intersections correspond to solutions of (3.51). Changing s merely corresponds to shifting $f(c)$ up and down. This means there is a critical value s_c such that the two curves just touch. For lower values of s there is no solution, for larger values there are two solutions. Thus if the solutions are plotted with s and c on the axes, one obtains the bifurcation diagram shown on the right of Fig. 3.13, known as a saddle-node bifurcation.

To find s_c, note that

$$f'(c) = \frac{2^{1/4}s}{2(\sqrt{a}-c)^{3/2}} = 1$$

at the bifurcation. Since Eq. (3.51) must also be satisfied, we find

$$c_c = \frac{2}{3}\sqrt{a}, \quad s_c = 2^{3/4}\left(\frac{\sqrt{a}}{3}\right)^{3/2}. \tag{3.52}$$

As a caveat we reiterate that the simplified theory of Eq. (3.49) presented here is by no means systematic, but nicely illustrates the mechanism of instability.

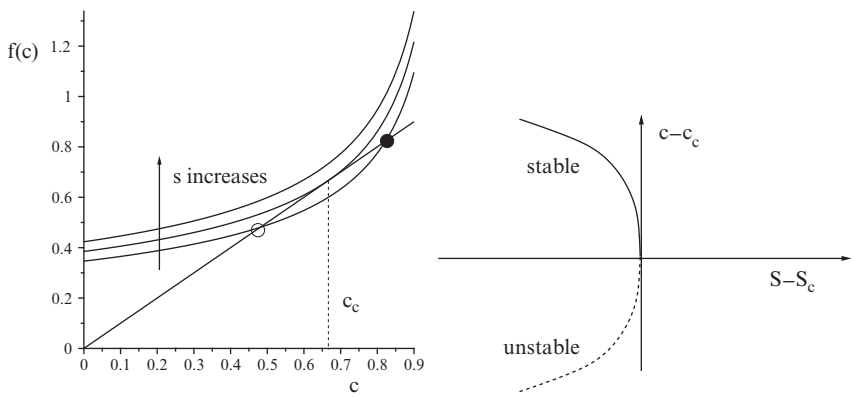

Fig. 3.13 (Left) Construction of the solution; the solid circle marks the stable solution, the open circle the unstable one. (Right) The bifurcation diagram.

For $s > s_c$ there are two solutions, the larger one of which (as shown in the upper branch of the bifurcation diagram) is stable, while the smaller one is unstable. Namely, on the lower branch upon increasing the control parameter s, c increases. This means that the cusp profile $H - H_c$ becomes *narrower*, increasing the effect of the gas further: this is an unstable situation. On the other hand, on the upper branch, the situation is reversed, and upon increasing s the system is brought back to its original state. Thus the solution corresponding to a narrower channel is stable, the other unstable. This is the typical situation for a saddle-node bifurcation, which is found in many systems. For example, the entrainment of a liquid film by a *solid* plate is governed by the same type of bifurcation [4].

Combining Eq. (3.44) and Eq. (3.50), we find that

$$Ca_c = C - \frac{2 \ln 10}{3\pi} \log_{10} \lambda. \tag{3.53}$$

The same quantities are plotted in Fig. 3.14. Unfortunately, the slope from a fit to the data is about -0.22, smaller than expected from Eq. (3.53).

3.3.4 Creation of a sheet

After the bifurcation, a sheet of the outer fluid (air) shoots out from the cusp tip. The simplest experiment to analyze this is that of a jet falling into a pool, illustrated in Fig. 3.15. In the absence of the upward pull 2γ the profile relaxes to a gravity-capillary balance. The jet enters smoothly, lubricated by the air. Thus the solution falls into two parts, which we treat separately. In the end, the two pieces need to be stitched together in a consistent fashion. This procedure is known as "matched asymptotics."

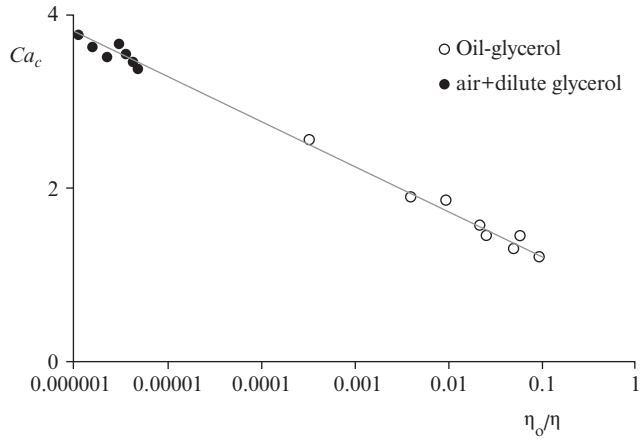

Fig. 3.14 The critical capillary number Ca_c for various combinations of liquids as well as liquids and air [10]. The viscosity of the outer fluid is η_0, so $\lambda = \eta_0/\eta$. Lorenceau, E., Restagno, F., and Quere, D. (2003). Fracture of a viscous liquid. *Phys. Rev. Lett.*, 90, 184501.

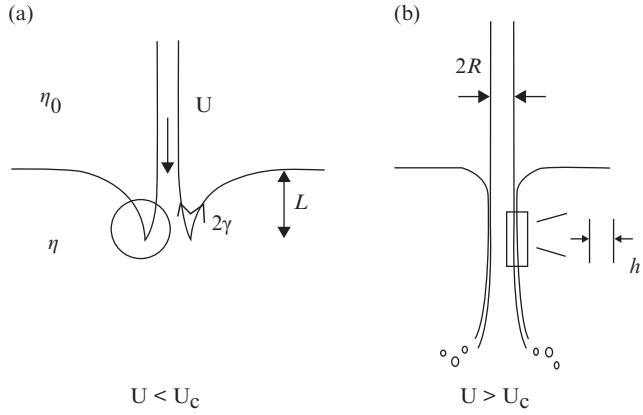

Fig. 3.15 A schematic of the transition shown in Fig. 3.2. Below the transition, a sharp cusp is observed. Above it, a cylindrical sheet of air penetrates the fluid.

3.3.4.1 Thin film (inner solution)

In the spirit of lubrication theory, we expand the velocity field in the "thin" direction, y (see Fig. 3.16 (right)):

$$u = -U + by + \frac{p'}{2\eta_0} y^2.$$

The jet entering at speed U is taken as $y = 0$. Near the point $x = 0$, where the jet enters the pool, the fluid in the pool is still stationary and thus $u(h) = 0$. It thus follows that $b = U/h - p'h/(2\eta_0)$ and the velocity field becomes

$$u = U\left(\frac{y}{h} - 1\right) - \frac{p'}{2\eta_0}\left(y^2 - yh\right).$$

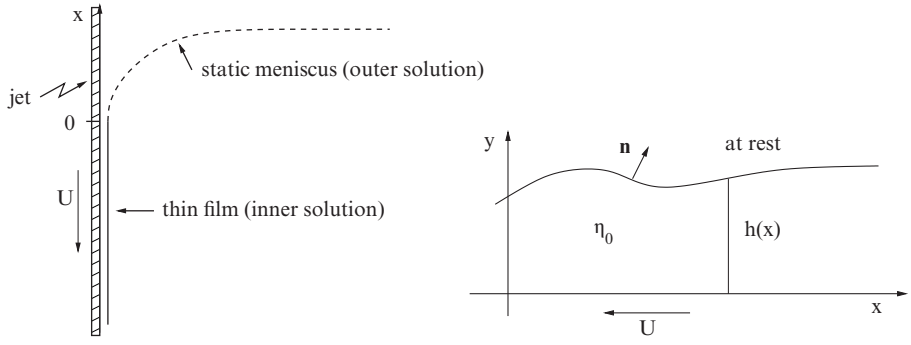

Fig. 3.16 (Left) The structure of the plunging jet problem. The outer fluid (air) forms a thin film, matched to an outer meniscus. (Right) The lubrication problem for the air film.

Finally, from the normal stress boundary condition at the top of the film we have $p = \gamma\kappa = -\gamma h''$.

The *flux* q through the film is

$$q = -\int_0^h u dy = \frac{Uh}{2} + \frac{p' h^3}{12\eta_0},$$

and so the lubrication equation can be written in the form

$$h''' = \frac{12Ca_0}{h^3}\left(\frac{h}{2} - \frac{q}{U}\right) \tag{3.54}$$

where $Ca_0 = U\eta_0/\gamma$ is the capillary number based on the air viscosity η_0. In the limit of small Ca_0 Eq. (3.54) has a similarity solution

$$h = Ca_0^\alpha H(\xi), \quad \xi = x/Ca_0^\beta, \tag{3.55}$$

with

$$\frac{q}{U} = QCa_0^\alpha.$$

Plugging this into Eq. (3.54), the terms are of the same order in the limit $Ca_0 \to 0$ if $\alpha - 3\beta = 1 - 2\alpha$ or $\beta = \alpha - 1/3$ and the similarity equation becomes

$$H'''(\xi) = \frac{12}{H^3}\left(\frac{H}{2} - Q\right). \tag{3.56}$$

Note that since $\beta < \alpha$, the solution is flat in the limit $Ca_0 \to 0$, making the use of the lubrication theory consistent.

The boundary conditions on Eq. (3.56) are such that for $\xi \to -\infty$ the solution approaches a flat film: $H(-\infty) = H_f$ and $Q = H_f/2$. On the other hand in the outer limit toward the meniscus (see Fig. 3.16) the film thickness grows quadratically, which can be confirmed from an analysis of Eq. (3.56). Thus in the limit $\xi \to \infty$ (the outer limit), H has the expansion

$$H = a\xi + b\xi^2,$$

where the constant a can be absorbed into a shift of ξ. Below we will match the quadratic growth for $\xi \to \infty$ to the outer solution. To that end we need a connection between b and the film thickness H_f, which we obtain by integrating Eq. (3.56) numerically from the film toward the outer solution.

First, we rescale Eq. (3.56) according to $g = H/H_f$ and $\eta = \xi 6^{1/3}/H_f$ to obtain

$$g_{\eta\eta\eta} = \frac{1}{g^3}(g - 1). \tag{3.57}$$

To understand the parameters involved, we expand around the film solution: $g = 1+\epsilon$. Plugging this into Eq. (3.57), one obtains the linearized equation

$$\epsilon''' = \epsilon.$$

Thus in the neighborhood of the film we have the solution

$$g = 1 + a_1 e^{\xi} + e^{-\xi}\left[a_2 \cos\left(\frac{\sqrt{3}\xi}{2}\right) + a_3 \sin\left(\frac{\sqrt{3}\xi}{2}\right)\right].$$

But for this solution to converge into a film in the limit $\xi \to -\infty$, the amplitudes a_2 and a_3 must vanish. In addition, the amplitude a_1 can be absorbed into a shift in ξ so there is really no free parameter.

This makes the numerics very simple: we solve Eq. (3.57), starting with the initial condition $g = 1 + e^{\eta_i}$, where η_i is sufficiently negative for the linearized version of the equation to be valid. We then integrate forward to a large positive value of η; we see from Fig. 3.17 that g behaves asymptotically like $g \approx (0.643/2)\eta^2$ and thus

$$H \approx \frac{2.123}{2H_f}\xi^2, \quad \xi \to \infty. \tag{3.58}$$

3.3.4.2 Meniscus (outer solution)

As the film of air enters the pool the free surface has to deform from its horizontal equilibrium to a vertical slope, where it merges with the air film, see Fig. 3.18. The

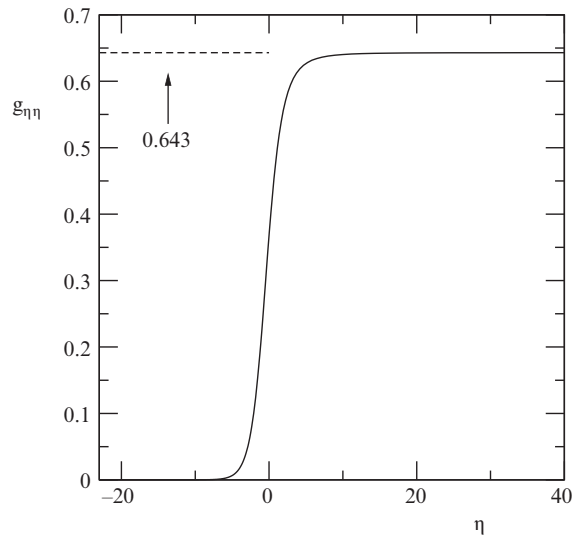

Fig. 3.17 Plot of $g_{\eta\eta}$ as obtained by integrating Eq. (3.57) forward. The asymptotic value of the second derivative is 0.643.

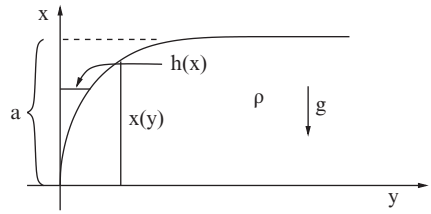

Fig. 3.18 Schematic of the meniscus joining the pool and the film.

typical length scale of this part of the solution is the capillary length $l_c = \sqrt{\dfrac{\gamma}{\rho g}}$. Note that the deformation of the free surface has changed from being controlled by viscosity to a surface tension–gravity balance. The reason is that the air film lubricates the entry of the jet, isolating the jet from its exterior. As a result, the exterior remains essentially unforced.

A balance of hydrostatic pressure and capillary pressure (in units of l_c) gives (see Fig. 3.18):

$$p_h = a - x = -\frac{x''}{(1 + x'^2)^{3/2}}.$$

Integrating, we obtain

$$\frac{(x-a)^2}{2} + \frac{1}{(1+x'^2)^{1/2}} = A \equiv 1,$$

since $x' = 0$ for $x = a$. At the "contact line" $x = 0$ where the meniscus joins the sheet we have $x' = \infty$, and so $a = \sqrt{2}$ and the curvature is $\kappa = \sqrt{2}$. Thus a local description of the outer solution near $x = 0$, now written as a function of x, is

$$h(x) = \frac{\kappa}{2}x^2 = \frac{x^2}{\sqrt{2}}. \tag{3.59}$$

3.3.4.3 Matching

Now we make sure that the inner and the outer solutions agree, i.e., that the asymptotics in Eq. (3.58) (the inner solution as it evolves toward the outer solution) have the same functional form as Eq. (3.59) (the outer solution as it reaches the film). This is indeed the case, since both functional forms for $h(x)$ are parabolae. To compare the prefactors we have to convert both descriptions to the same variable using the scaling in Eq. (3.55). Thus we obtain

$$h(x) = \frac{2.123 Ca_0^{\alpha}}{2H_f} \frac{x^2}{Ca_0^{2\alpha - 2/3}} = \frac{x^2}{\sqrt{2}}.$$

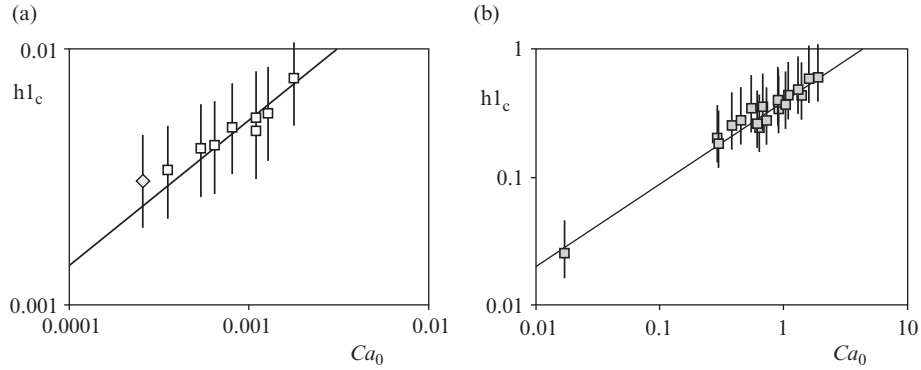

Fig. 3.19 Experimental measurements of the sheet thickness [9]. Lorenceau, E., Quere, D., and Eggers, J. (2004). Air entrainment by a viscous jet plunging into a bath. Phys. Rev. Lett., 93, 254501. (Left) Thickness of an air film entrained by a glycerol jet. (Right) Thickness of oil films entrained by a glycerol jet surrounded by oil, impacting a glycerol bath. The fit corresponds to Eq. (3.61) with a prefactor of 0.5.

For this to be true in the limit $Ca_0 \to 0$ we firstly must have $\alpha = 2/3$ to make the left-hand side Ca_0-independent. Comparing the remaining prefactors, we obtain the *matching condition*

$$H_f = \frac{2.123}{\sqrt{2}} = 1.501. \tag{3.60}$$

In conclusion, and restoring units, the film thickness is

$$h = 1.501 l_c Ca_0^{2/3}. \tag{3.61}$$

The scaling is well confirmed by experimental measurements (see Fig. 3.19, solid lines), but the prefactor is 0.5, considerably smaller than predicted. The reason for the discrepancy is currently unknown. Another issue that remains to be studied is the break-up of the sheet into bubbles, which occurs at a well-defined position along the sheet. What is the mechanism of the break-up, and what is the size (distribution) of the bubbles?

3.4 Conclusions

In this series of lectures, we have looked at two different types of free-surface singularities: a time-dependent singularity, which leads to the formation of a bubble, and a stationary cusp singularity, which leads to the formation of a sheet of air. In this, we were guided by two key ideas: Scaling and Universality. As a result, we were able to characterize both singularities in terms of scaling exponents, as well as a universal scaling function. We also found that simple geometrical ideas sometimes help us to understand the solution to a difficult partial differential equation.

References

[1] Barenblatt G. I. *Similarity, Self-Similarity, and Intermediate Asymptotics*. Cambridge: Cambridge University Press; 1994.
[2] Doshi P., Cohen I., Zhang W. W., Siegel M., Howell P., Basaran O. A., et al. Persistence of memory in drop breakup: The breakdown of universality. *Science*. 2003; 302: 1185.
[3] Eggers J. Air entrainment through free-surface cusps. *Phys. Rev. Lett.* 2001; 86: 4290.
[4] Eggers J. Existence of receding and advancing contact lines. *Phys. Fluids.* 2005; 17: 082106.
[5] Jeong J.-T. and Moffatt H. K. Free-surface cusps associated with a flow at low Reynolds numbers. *J. Fluid. Mech.* 1992; 241: 1–22.
[6] Joseph D. D., Nelson J., Renardy M., Renardy Y. Two-dimensional cusped interfaces. *J. Fluid Mech.* 1991; 223: 383–409.
[7] Lafaurie B., Nardone C., Seardovelli R., Zaleski S., Zanetti G. Modelling merging and fragmentation in multiphase flows with SURFER. *J. Comput. Phys.* 1994; 113: 134.
[8] Landau L. D. and Lifschitz E. M. *Fluid Mechanics.* Oxford: Pergamon; 1984.
[9] Lorenceau E., Quere D., Eggers J. Air entrainment by a viscous jet plunging into a bath. *Phys. Rev. Lett.* 2004; 93: 254501.
[10] Lorenceau E., Restagno F., Quere D. Fracture of a viscous liquid. *Phys. Rev. Lett.* 2003; 90: 184501.
[11] Muskhelishvili N. I. *Some Basic Problems of the Mathematical Theory of Elasticity*. Groningen, The Netherlands: P. Noordhoff; 1953.
[12] Wegner F. J. Corrections to scaling laws. *Phys. Rev. B.* 1972; 5: 4529.